Chapter 2

Synthesis and characterization techniques

This chapter deals with details of samples preparation methods and an overview of employed different characterization techniques. The physical properties of any nanostructured materials/systems strongly depend on the crystal structure, size & shape, and distribution of nano crystallites. As we have already discussed that the crystal structure, composition, and surface topology of LNMO are sensitive to the synthesis route and conditions. Different crystal structures such as orthorhombic, monoclinic, & rhombohedral, and cation ordering/disordering co-exist with different synthesis conditions. The cations ordering influences the magnetic, optical, and electric properties, etc. Apart from these, oxygen stoichiometry or vacancies are also dependent on the synthesis route and conditions. Thus, the selection of synthesis routes and conditions can modify the collective properties of these systems.

2.1 Synthesis/Growth method

We have adopted solid-state and sol-gel synthesis routes to synthesize the LNMO nanomaterials. Along with high-quality precursors and calcination/sintering temperatures, atmosphere, pressure, and heating rate could modulate defect and cation ordering in such systems. The solid-state chemical route and sol-gel method were adopted to synthesize the LNMO nanoparticles. The overview of synthesis routes and conditions will be discussed in further sections.

2.1.1 Solid-state synthesis route

The solid-state synthesis method is well proven and an excellent technique for complex oxide synthesis [72]. In this technique, the precursor materials were taken in solid form and mixed by ball milling that reduces the particle size as well mix the powders uniformly. After milling, the powder was calcined at different temperatures (500-2000 K) for initial phase formation. This technique depends on thermodynamic and kinetic factors [73]. Thermodynamically, the reaction is possible in solid form by changing the free energy, which depends on various kinetic factors. The final phase formation also depends on the size of a particle because lower size particle has higher surface energy and diffusion rate [74]. In this thesis work, the LNMO nanopowders were synthesized using solid-state synthesis route for different milling times. Figure (2.1) represents the flow diagram of the solid-state synthesis route adopted for the LNMO nanoparticles. In total, we have synthesized three samples of LNMO milling for different times 10, 15, and 25 h. The details of each step are described as follows:

• **Raw materials:** The starting materials or precursors are high-purity oxides (more than 99 %) to synthesize a final oxide (LNMO) material. Raw materials were made free from moisture and other volatile impurities.

• **Stoichiometric amount:** Stoichiometric amount or proportioning is most important in the solid-state route. Proportioning is defined as the required accurate amount of powders to get the desired compound. The amount of raw powders were estimated on molecular weight basis as shown below.

$$La_2O_3 \; + \; MnO_2 + \; NiO \; \longrightarrow \; La_2NiMnO_6$$

$$(325.81g) \;\; (89.94g) \;\; (74.69g) \;\;\; (487.4388g)$$

- La_2O_3 required amount for 1 g = (325.81/487.4388) = 0.6684 g
- NiO required amount for 1 g = (74.692/487.4388) = 0.1532 g
- MnO_2 required amount for 1 g = (89.936/487.4388) = 0.1845 g

These calculations are based on 100 percent pure raw powders. If the raw powder is not completely pure then we have to do assay corrections that based on the purity fraction.

• **Ball milling:** Ball milling was utilized for two basic purposes (i) reduction in particle size and (ii) uniform mixing of precursor. Ball milling is a type of mechanical grinding that is commonly used to mix and grind powders materials into a smaller uniform powders [75]. It is made up of a hollow cylindrical container that revolves around its center and is partly filled with stainless steel or ceramic balls. The energy released from impact and attrition between the balls (grinding or milling medium) during the ball milling results in

size reduction. This method comes with a lot of benefits that include cost-effectiveness, reliability, reproducibility, and different conditions applicability. The main disadvantages are the requirement of purification and irregular shape formation.

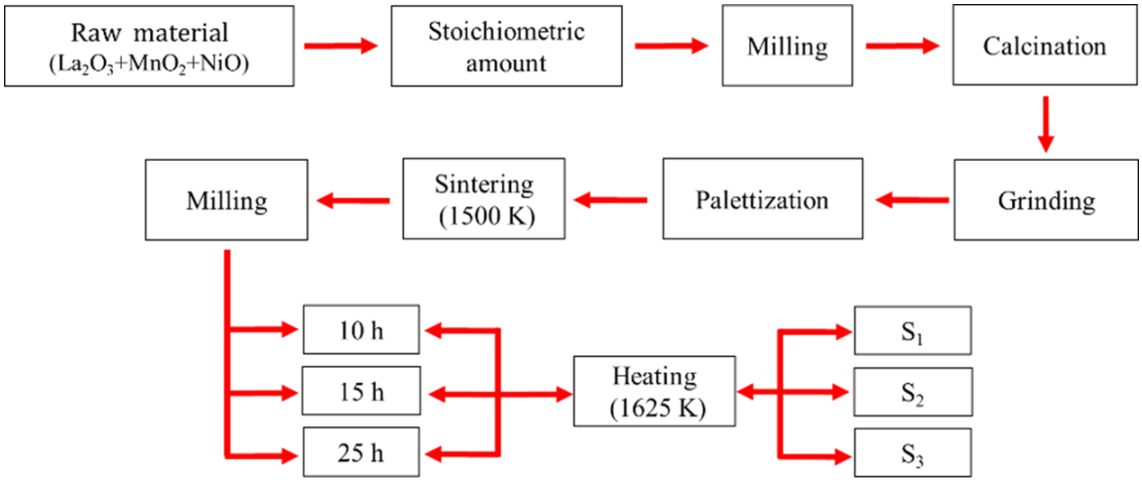

Fig. 2.1 Flow chart of solid-state synthesis route adopted for the synthesis of LNMO crystallites.

• **Calcination:** Calcination is defined as primary heating for required phase stablization. At different temperature regions, chemical decomposition and the reaction takes part such as decomposition, and removal of volatile materials and hydroxy and crystalline water. The milled powders are calcined at different temperatures that depend on specific powder and reaction temperature. The rate of diffusion depends on particle size, heat flow rate, and calcination temperature. The higher diffusion rate improves uniformity of the compound and reduces the fraction of secondary phase or unwanted phase.

• **Palletization:** The process by which powders are converted into pallets is known as palletization. The pallet is formed by different technologies such as hydrostatic press and isostatic press. Mostly pallet is formed to increase the density of powders, due to some properties depending on strength and void fraction. The pallet is synthesized by adding some binder (such as polyvinyl alcohol) in milled powders, then powders are pressed through different sizes, and shapes of dye [73, 74]. These compaction parameters depend on the rheology of the powder, shape, and size of the powder. The hydrostatics pressure is calibrated by the maximum density achieved. The green pallet (before sintering) should be free from any crack and void otherwise it may break during sintering.

• **Sintering:** Sintering is a process of densification at high temperatures due to the grain growth mechanism [73, 74]. It is a high-temperature heating process to develop a stable chemical bond between the atoms. The pallet is sintered at a higher temperature after the binder has been removed at a low temperature. Sintering directly at high-temperature

may rapidly generate volatile gases which may generate cracks in the pallet. The sintering temperature is always below or less than the melting temperature (solid-state sintering), which depends on the specific powder. The particles go through several diffusion (grain boundary and volume) processes during sintering, and these mechanisms are influenced by temperature [74]. Along with temperature, other variables that affect diffusion during sintering include particle size and distribution, material composition, and the sintering environment [74]. The activation energy necessary for diffusion processes is directly impacted by temperature control, which makes it crucial. Engineers and scientists can tune the sintering conditions to produce the desired densification, grain growth, and material qualities by altering the temperature.The ideal temperature profile may change based on the desired qualities of the finished product since different materials have different sintering temperature ranges.

The following discussion concludes the different steps utilized during sample synthesis. The adopted route of solid state route is shown in Fig. (2.1). In order to fracture, deform, and grow in refined facets of microscopic crystallites, a sintered LNMO pellet was smashed up into small particles and ball-milled in ethanol for 10 h (S_1), 15 h (S_2), and 25 h (S_3). The cation mixing and densification processes are both assisted by the milling at certain times.

2.1.2 Sol-gel synthesis route

This is a kind of wet chemistry route, and there are ample reports available in the literature [76, 77]. This technique is a bottom-up approach to materials synthesis where individual ions coalesce to form a compound. Most compounds synthesize at lower temperatures compared to solid-state routes, so this belongs to the energy-efficient route. The different stages of the adopted sol-gel synthesis route were shown in Figure (2.2). We synthesize the different Sm-doped samples $La_{2-x}Sm_xNiMnO_6$ (where $x = 0, 0.1, 0.2, 0.5$). The synthesis of Sm-doped $La_{2-x}Sm_xNiMnO_6$ (where $x = 0, 0.1, 0.2, 0.5$) via high purity precursors lanthanum nitrate ($La(NO_3)_3.6H_2O$), samarium nitrate ($Sm(NO_3)_3.6H_2O$), nickel nitrate ($Ni(NO_3)_2.6H_2O$), manganese acetate ($C_4H_6MnO_4.4H_2O$). The stoichiometric amount of precursor compounds was dissolved in 2-methoxy ethanol to make transparent solutions. These solutions were then combined in the appropriate ratio. The mixed solutions were agitated at room temperature for 2 hours to produce a clear homogeneous solution. This solution (sol) was cured at 340 K for 12 hours to obtain the gel. Finally, the gel was dried at 470 K to extract the powder calcined at 1050 K for 5 hours to get the pure phase of $La_{2-x}Sm_xNiMnO_6$ (where $x = 0, 0.1, 0.2, 0.5$). The final particle size obtained from this route depends on the calcination temperature, time, and pH of precursor solutions.

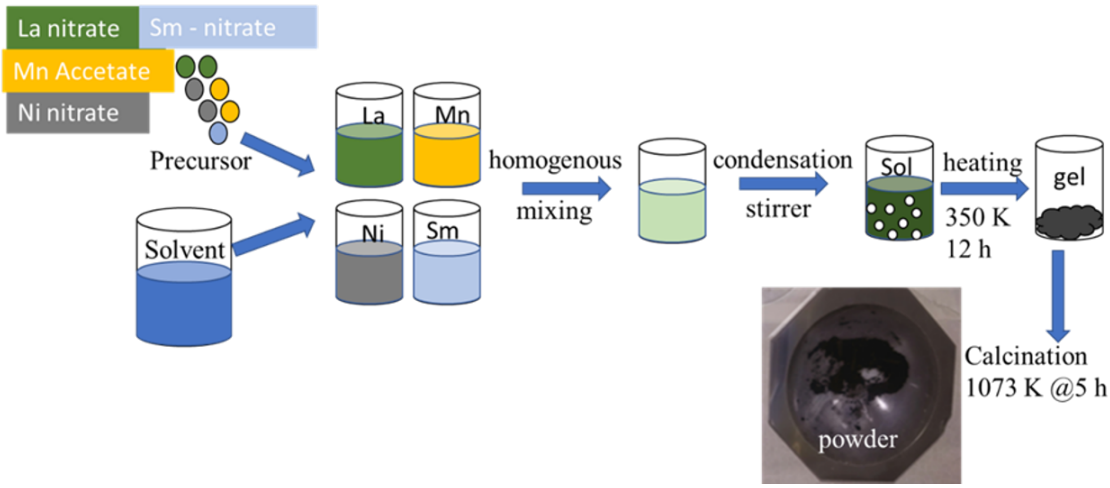

Fig. 2.2 Flow chart of sol-gel synthesis route adopted for the synthesis of LNMO crystallites.

2.2 Characterization techniques

It is impossible to comprehend the scientific and technological benefits of generated materials unless they are characterized. Characterization is the process of learning about a material's properties, compositions, morphology, crystal structure, and magnetic structure. It is critical for identifying a material's physical and chemical properties and for the proper implementation of substances in scientific applications or industries. The characterization techniques used in this thesis are briefly discussed in this section: X-ray diffraction, scanning electron microscopy, energy dispersive X-ray analysis, transmission electron microscopy, X-ray photoelectron spectroscopy, Raman spectroscopy, electron spin resonance, and magnetic property measurement system (magnetometry). A brief discussion of these characterization tools was described below.

2.2.1 X-ray diffraction

Powder X-ray diffraction (XRD or PXRD), which creates a distinct diffraction pattern fingerprint, is the most commonly used polycrystalline material phase confirmation technique. XRD is one of the most versatile approaches for studying crystal structure, phase, and other structural characteristics such as average grain size, strain, crystallinity, and crystal defects in bulk materials (solid solution) and thin films. Determining the crystal structure is an important aspect of materials characterization since the physical characteristics of solids are heavily dependent on the atomic arrangement and symmetries. For a full discussion and the well-established theory of diffraction, as well as the experimental setup of a modern laboratory diffractometer, which is discussed in numerous textbook [78–81].

The technique is based on the fact that X-rays have a wavelength in the same range as the interplanar distance (d) between the planes of a crystal system. When X-rays are incident on a crystal, they are scattered coherently by the lattice planes, resulting in a diffraction pattern.The foundation of X-ray diffractometry (XRD) is Bragg's law, which stipulates that incident X-rays are diffracted from a number of equally spaced lattice planes in the crystal that constructively interact. The integral multiple of their path difference is the X-ray wavelength. Bragg's law specifies the following conditions for constructive diffraction:

$$n\lambda = 2d_{(hkl)}\sin(\theta) \tag{2.1}$$

where λ is the wavelength of the incident X-ray, d_{hkl} is the interplanar distance between planes with (hkl) Miller indexes, and n represents the order of diffraction. Figure (2.3) is a schematic diagram that demonstrates Bragg's law. .

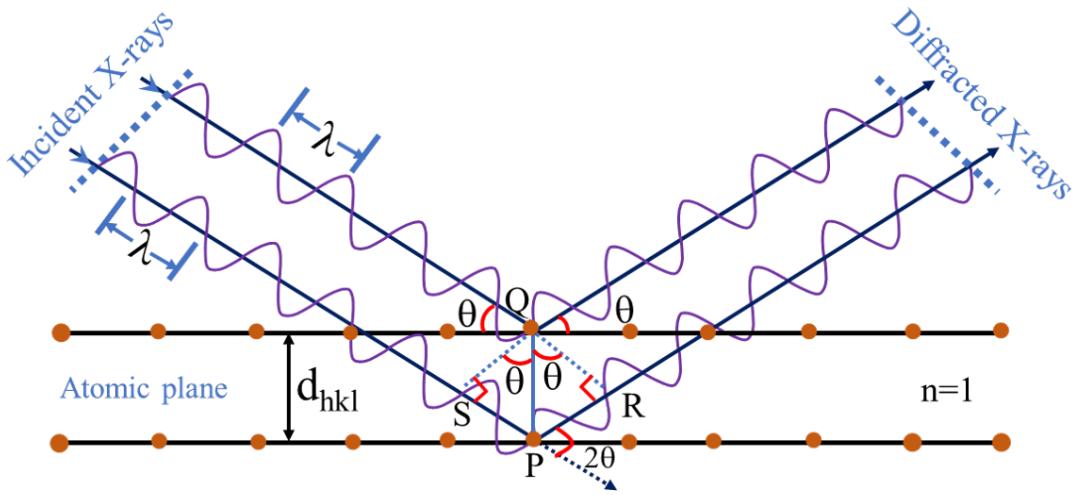

Fig. 2.3 Schematic illustration of XRD and Bragg's law.

When a convergent monochromatic X-ray beam is focused on a powder sample, the sample diffracts the X-rays in a cone-like pattern of radiation. This pattern is determined by the internal structure of the powder sample. Elastic scattering causes the highest intensity of scattered radiation to be in the directions where the magnitude of the incident particle's momentum vector is added to a vector belonging to the polycrystalline reciprocal lattice. These directions are known as Bragg peaks or Bragg locations and can be assigned a set of Miller indices. The real space lattice can be computed as the reciprocal space's Fourier transform. Each peak location is subject to Bragg's law. To obtain the X-ray patterns of samples, an X-ray diffractometer (Rigaku) with monochromatic Cu K_α = 1.54056 Å was employed. The diffraction patterns were recorded from 10° to 100° with a step size of 0.02

degree/s. A typical representation of XRD data is in the form of intensity (count/s) and 2θ. The positions and intensities of the Bragg peaks reveal essential information about the crystal structure and properties of the material under investigation.

The XRD data of the samples were analyzed to confirm their phase purity by comparing them with standard data from the Joint Committee on Powder Diffraction Standards (JCPDS). The Rietveld refinement method, implemented in the FullProf program, was used to analyze the diffraction patterns [80, 82]. This method not only determines the phase purity of the samples, but also provides crystal structure information such as lattice parameters, atomic positions, occupancy, bond-lengths, and bond angles [83]. A non-linear least square technique was used to minimize the difference between the experimental and calculated XRD patterns during the refinement process. A linear interpolation was used to refine the background, and a Pseudo-Voigt function was used to optimize the peak shape. The refinement mainly involved varying global parameters such as background polynomial coefficients, scaling factor, FWHM parameters (u, v, w), and lattice parameters (a, b, c). Furthermore, the fractional atomic coordinates (x, y, z), isotropic parameters, and occupancy values were also defined. The multiplicity of the Wyckoff position divided by the maximum multiplicity of the same space group equals occupancy. Reliability factors such as R_p (profile factor), R_{wp} (weighted profile factor), R_e (expected weight factor), and χ^2 (reduced chi-square) were used to evaluate the quality of Rietveld refinement. The bond lengths/interatomic distances and angles were calculated using the Vesta software, part of the Full Prof. suite [84].

2.2.2 Scanning electron microscopy

Scanning electron microscopy (SEM) is a highly sophisticated imaging method that uses a high-energy (1.0 keV) electron beam to examine the morphology, fractured components, foreign particles, and residues on a very fine scale. Aside from that, the main application of SEM is to acquire high magnification topographic images of 10 - 10000 X by using electrons (instead of light) to obtain an image, making the SEM much more adaptable [85, 86]. SEM employs two kinds of electron sources: thermionic emitters and field emitters. The thermionic emitter uses electrical current to heat the filament until the heat exceeds the work function, resulting in highly energetic electrons escaping the material surface. In comparison, the field emitter, known as the cold cathode emitter, generates an electron beam using a large electrical voltage gradient. The thermally assisted Schottky emission mode is used by the electron gun, which is made of tungsten with a zirconium oxide coating (ZrO_2/W). With the use of a high-energy electron and a narrower probing

beam, this kind of gun produces better spatial resolution, less sample damage, and reduced charge.

The electrons are accelerated using the voltage difference between the electron gun (acting as a cathode) and anode of the order of 0.5-30 eV. The instrument's high vacuum environment ceases electron scattering and discharge. Electromagnetic lenses focus the primary electrons into a narrow beam that impinges on the sample's surface, producing ionization of surface atoms and emission of loosely bound secondary electrons. A high-efficiency annular in-lens ac-detector captures the secondary electrons, and their intensity is compared to that of the incident primary electron beam to generate an image of the specimen surface. The SEM experiment generates a topographic picture by moving a finely concentrated electron beam across the surface of a specimen.

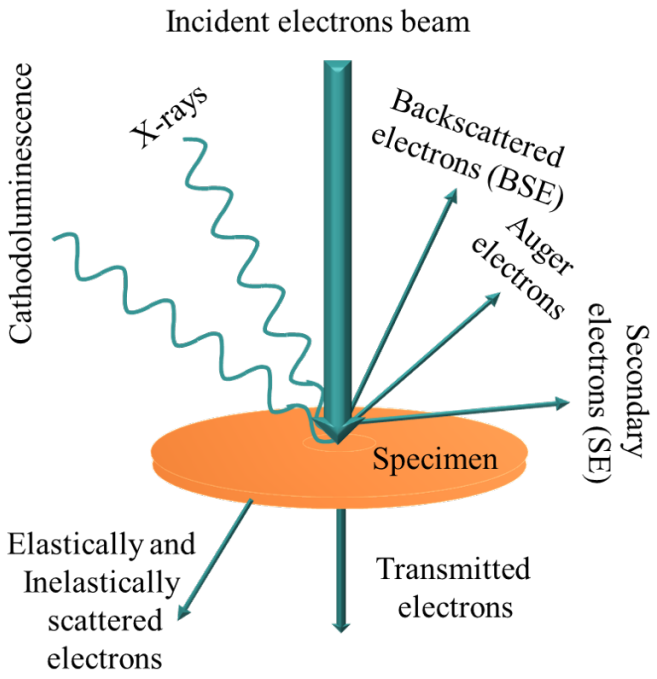

Fig. 2.4 Schematic diagram of various outcomes of electron beam interacting with the specimen.

This beam irradiates a small area or microvolume of the specimen being inspected, producing a variety of signals unique to the type of interaction between the incident electrons and the specimen material, such as X-rays, cathodoluminescence, backscattered electrons, auger electrons, and secondary electrons (see Figure (2.4)). These instructive signs are used to investigate various specimen traits such as surface topography, morphology, and composition. The signals are obtained from a precise emission volume within the specimen, and the secondary and backscattered electron signals are especially useful for 3-D

imaging because they show surface topography variations. Surface atoms are ionized when the beam strikes the specimen, resulting in the emission of loosely bonded electrons known as secondary electrons. Other signals released in addition to secondary electrons include backscattered electrons (BSE) from the bulk of the sample, transmitted electrons, characteristic X-rays, and specimen current. To capture these signals, specialized detectors are needed, and it is uncommon for all detectors to be integrated into a single machine. Because of particular beam energy choices, secondary electron emission is confined to a narrow area near the beam impact, allowing images to be viewed at a resolution equal to the size of the electron beam. Backscattered and secondary electron signals create a shallow depth of field and a shaded relief effect, resulting in three-dimensional images.

In this study, the samples were coated with an extremely thin layer (0.5 to 1.5 nm) of gold to create a conductive surface. The imaging of the coated samples was performed using a field emission gun-based scanning electron microscope (FE-SEM) of SIGMA, ZEISS. For image processing and analysis, a Java-based imaging program called ImageJ was utilized [87]. The FE-SEM images were processed using this software to extract relevant information and analyse the morphological features of the samples. In the following part, a study has been made to analyze the X-ray radiation emitted from the specimen. It gives qualitative and quantitative elemental results from the area of concern of the specimen. Characteristic X-rays have been used which is usually a result of electron bombardment in SEM imaging.

2.2.3 Energy dispersive X-ray spectroscopy

Energy dispersive spectroscopy (EDS) is a widely used technique for the analysis of a sample's chemical composition, elemental fraction, and homogeneity. We can detect emitted X-rays with electron beam bombardment. It is also known as energy dispersive X-ray analysis (EDAX). These emitted X-rays are specific to the elements found in the sample, and their intensity is proportional to their concentration. The EDAX system then separates and analyses these X-rays based on their energies, producing a full spectrum that reveals the sample's elemental mapping and composition. EDAX can also be used for elemental mapping, which visualizes the spread and concentration of elements within a sample. EDAX is a non-destructive method that uses a Z (atomic number) $\geqslant 11$ to rapidly calculate proportion of all constituent elements. Characterization (studying features as tiny as 1 μm or less) is based on the fundamental premise that each chemical constituent has a unique electronic structure, resulting in X-rays of definite energy fundamental characteristic of an element, enabling chemical identification.

2.2.4 Transmission electron microscopy

The transmission electron microscope (TEM) is a versatile technique for the structure and morphology of materials at high magnification. The morphological information such as shape, size, and distribution of constituents is characterized by TEM. Techniques including HRTEM (high-resolution TEM), selected area electron diffraction (SAED), and elemental mapping with extra units like EDX (energy dispersive X-ray analysis) and elemental mapping can be utilised as per the requirements [88, 89].

TEM uses an electron cannon, a vacuum system, electromagnetic lenses, a high-voltage generator, recording devices, and related electronics to function. All of these components work together to allow electrons to pass through the material, concentrate and manipulate the electron beam, and record and view the resulting image in a TEM. Electrons with a shorter wavelength are utilized in TEM, which allows for high-resolution imaging at the atomic level. A well-focused electron beam produced by an electron cannon assembly and electromagnetic condenser lenses is accelerated by an anode that is normally at a cathode-to-anode energy difference of 100 keV. The condenser aperture blocks un-collimated electrons and limit the beam. When a collimated high-energy electron beam (200 keV or higher) hits the specimen, and scatters according to its thickness and electron transparency. An image is produced on a phosphor screen or charge-coupled device (CCD) camera when the objective lens transmits and focuses a piece of the scattered electron beam that has altered phase and amplitude during scattering. The contrast can be improved by adjusting the objective aperture by preventing high-angle diffracted electrons. Data is gathered in transmission mode, with a sample geometry restriction of 100 nanometers or less [86].

Surface morphology (particle shape and size), lattice planes, distortion, and deformation were examined using TEM in this research. The sample was prepared by dispersing or dissolving nanoparticles in ethanol, then depositing a drop of this solution onto a carbon-coated copper grid to ensure the sample's conductance.

Data analysis

The shape and size distribution of the disseminated particles in the TEM micrograph is investigated. To ensure phase quality and crystallinity of the materials, the selective area electron diffraction (SAED) pattern is applied. The inverse of the diffraction pattern's radii is calculated and matched with interplanar spacing (d) in the reciprocal space of XRD data using WinPLOTR software.

High-resolution transmission electron microscopy

High-resolution transmission spectroscopy (HRTEM) is a special TEM imaging mode that produces high-resolution micrographs of a sample's crystallographic structure at the atomic length scale. An interference image is created by combining the transmitted and dispersed photons. HRTEM's phase-contrast image can be as tiny as a crystal's unit cell. It can generate images with a resolution of less than 1 Å at magnifications of more than 50 million times. Height, rotation center, orientation, defocus, astigmatism, and other factors all play a role in TEM and sample alignment. The electron gun is powered by a voltage of about 200 kilovolts. HRTEM's well-defined atomic planes are indexed by computing the d (interplanar distance) and compared to XRD data to establish phase purity at the nanoscale [90].

2.2.5 X-ray photoelectron spectroscopy

X-ray photoelectron spectroscopy (XPS) is widely used for analyzing the specimen's elemental composition, valence, and oxidation states. It is a surface sensitive technique and also known as electron spectroscopy for chemical analysis (ESCA).

In the middle of the 1960s, Kai Siegbahn and his research team at the University of Uppsala in Sweden developed the XPS technology, which is based on the photoelectric effect. XPS is based on the photoelectric effect, in which core-level electrons are stimulated by powerful X-ray photons with energies of hν. The following is an expression for the kinetic energy of the released electrons:

$$K.E. = h\nu - B.E. - \phi \tag{2.2}$$

where K.E. is the kinetic energy of the emitted electrons, hν is the energy of the incident X-ray photon, B.E. is the binding energy of the core level electron, and ϕ is the work function of the material. This relationship shows the dependence of emitted electron's kinetic energy on the energy of incident X-ray photons, the binding energy of inner shell electrons, and the work function of the material. Figure (2.5) Picturized ejection of core level electron due to interaction of X-ray. Binding energy refers to the energy required for the ejection of core-level electrons to the fermi level. With kinetic energy measurement of ejected electrons, XPS can show the chemical composition and electronic structure of the specimen's surface. XPS is a technique used to identify the electronic state of a material by analyzing the kinetic energy of photoelectrons emitted from its surface. The XPS spectrum is plotted as the frequency of emitted electrons against their kinetic energy and intensity. The binding energy of each electronic states is in relation with fermi energy level. Kinetic

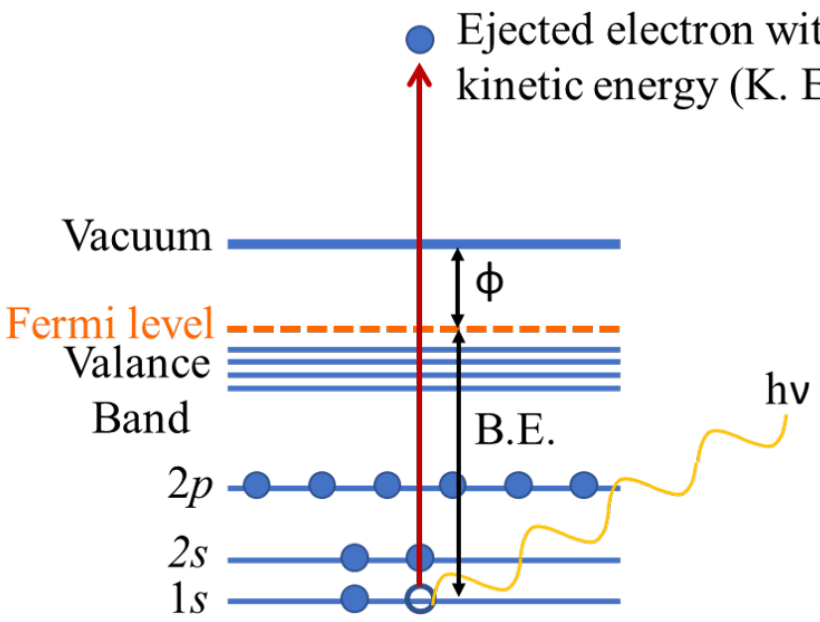

Fig. 2.5 Schematic diagram of photoelectron or principle of XPS.

energy distribution of photoelectrons tells about the electronic state energy distribution for a given photon energy.

However, photoelectrons may be scattered by adjacent electrons, plasmons, or phonons during the photoelectron emission process, resulting in a partial loss of energy. Because of strong electron-electron interactions, the scattering effect is more evident at low kinetic energies. As a consequence, the excited photoelectrons lose a significant amount of energy and are unable to pass through the specimen, resulting in undesirable secondary inelastic background intensity. This scattering effect restricts photoelectronic detection to a few tens of angstroms below the surface. It's crucial to remember that the scattering and attenuation effects have confined the detection depth in XPS to the vicinity of the surface. However, certain photoelectrons with enough kinetic energy can get past the work function barrier and the effects of scattering, enabling them to reach the detector. Usually, the top few nanometers of the material's surface are where these photoelectrons are released. XPS gives details about the elemental composition and chemical states of the material's surface by detecting and examining these photoelectrons that are emitted. In XPS experiments, the scattering and collisions of emitted electrons can negatively impact the detection of photoelectrons. However, the use of ultra-high vacuum conditions reduces such effects and allows for enhanced mean free paths of emitted electrons. Monoenergetic soft X-rays, such as those generated by Al-K_α (1486.6 eV) and Mg-K_α (1253.6 eV) radiation sources,

are preferred for exciting photoelectrons, and an electrostatic analyzer is used to analyse the excited photoelectrons.

In this study, K-Alpha model of Thermo Fisher Scientific was used to perform XPS measurements. The sample analysis chamber's vacuum level was kept at $\sim 10^{-9}$ Torr while the sample preparation chamber was evacuated to a pressure of $\sim 10^{-8}$ Torr. A survey scan was first conducted to collect the complete range of energy, followed by the selective recording of O-*1s*, Mn-*2p*, La-*3d*, Sm-*3d*, and Ni-*2p* core level spectra for precise elemental analysis and determination of sample composition. According to the C-*1s* peak with a center value of $\sim$284.8 eV, all core level XPS spectra were calibrated.

2.2.6 Raman spectroscopy

Raman spectroscopy is a method that uses light scattering to investigate the dynamic properties of atoms, ions, and molecules in a crystal. C.V. Raman and his study partner Krishan invented the technique in 1928, inspired by the Compton effect, in which X-rays are scattered by electrons. Raman's first experiments used sunlight and his naked eye as detectors, but the method has since been improved with sophisticated instrumentation, such as excitation sources and detectors.The majority of photons that are scattered when light passes through a molecule or crystal are elastically dispersed, which means they retain the same energy as the incident photons. However, a small fraction of the photons ($\sim$1 in 10^7) are inelastically scattered, resulting in a change in their wavelength due to changes in the rotational, vibrational, or electronic energy of the molecule. This inelastic scattering is known as the Raman effect or Raman shift, while elastic scattering is called Rayleigh scattering.

The Raman effect is explained by the deformation of molecules in an electric field of strength E, which causes an electric dipole moment (P) given by; P =αE (α is the polarizability). The Raman shift can be detected only if the derivative is non-zero with respect to Q. (normal co-ordinates). When electromagnetic radiation interacts with an atom or molecule, the electron clouds and bonds of the molecules are distorted, and the atom or molecule is excited to a virtual energy level from its ground state, causing it to become unstable. These excited molecules revert to a different stable state (rotational or vibrational) by releasing a photon and decreasing their energy. The difference in energy between the molecule's early and final stable states causes the frequency of the emitted photon to shift away from the excitation energy. If the end state has more energy, we get an emitted photon with a lower frequency than the excitation frequency, which is known as the Stokes shift. However, when the final state has lesser energy, we get an emitted photon of higher energy, and this shifting is known as the anti-Stokes shift. Figure (2.6)

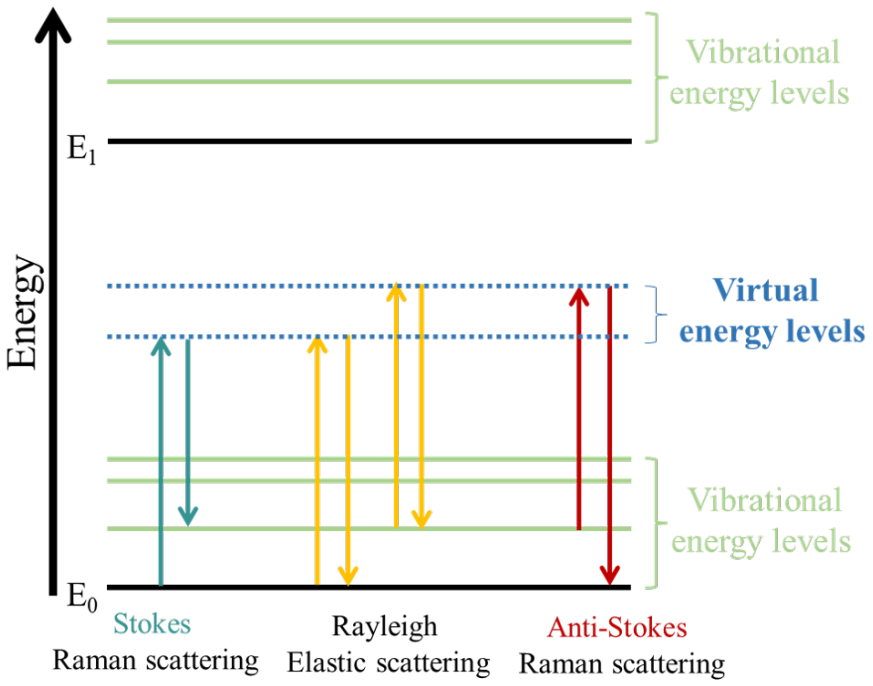

Fig. 2.6 Illustrate elastic and inelastic scattering via energy band diagram.

shows the different scattering-induced vibration energy band transitions. Raman spectra are typically characterized in terms of wave numbers in the inverse of length units. (cm^{-1}). Since its discovery in 1928, the method has seen numerous advancements, including the development of a good excitation source with advanced detectors and the commercial availability of Raman spectrometers. Raman spectroscopy has evolved into a novel method for probing the qualitative and quantitative dynamics of atoms/ions/molecules in crystals via light scattering.

In our study, we have used the Horiba LABRAM-HR spectroscope. Here, a monochromatic laser light of wavelength 472 nm, using a diode-pumped solid-state laser with a maximum power of 100 mW was used. To avoid heating and fluorescence of the specimen, only 50 % power was allowed to incident on the sample. The laser beam was focused at a much shorter working distance over a 50× long-distance objective connected with the Leica DM 2500 M microscope. The temperature of the system was controlled by a Linkam furnace type TS 1000 connected to a Linkam controller model T 95. To eliminate Rayleigh scattering, a notch filter was employed.

2.2.7 Electron paramagnetic resonance

Electron paramagnetic resonance (EPR) identifies transitions caused by electromagnetic radiations in a static magnetic field from electron spins to their various energy levels. It is also known as electron spin resonance (ESR). EPR is a spectroscopic tool that can detect the presence of material species that have an unpaired electron due to excitation to a higher energy state under a magnetic field by absorbing microwave frequencies. Unpaired electron spins in paramagnetic solids can be induced to transition between spin states by applying a magnetic field and providing microwave frequency electromagnetic energy. The magnetic moment associated with the spin, which can have one of two directions, controls how an external magnetic field interacts with an electron spin. When a magnetic field is applied, the spin states are split by a quantity proportional to the magnetic field. (Zeeman effect). The transition between two distinct energy levels is accomplished by absorbing a quantum of microwave radiation. Plank's rule states that electromagnetic radiation will be absorbed if and only if the following condition:

$$E = h\nu \tag{2.3}$$

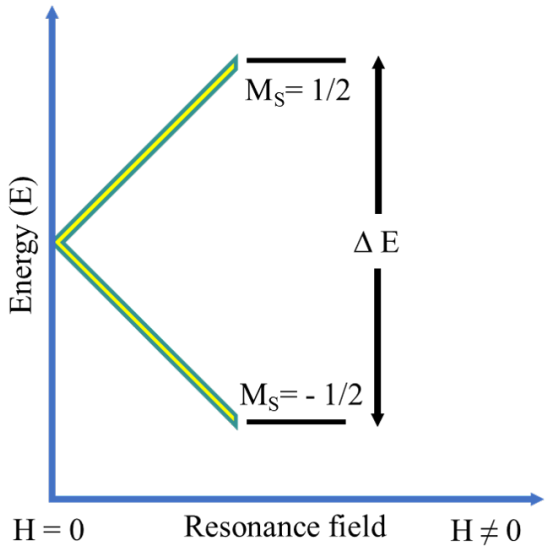

Fig. 2.7 Energy level diagram for two spin states as a function of applied field B.

where E is the difference in energy between the two states, h is Plank's constant and ν is the emission frequency. An electron moves from a lower energy state to a higher energy state as a result of this energy being absorbed. EPR spectroscopy employs gigahertz-frequency radiation. EPR spectroscopy is built on the spin of an electron and the magnetic

moment that goes along with it. The two potential spin states of an electron have different energies when it is exposed to a magnetic field. When the energy of the microwaves utilized in EPR spectroscopy corresponds to the energy difference between the two spin states, the resonance condition takes place. The phenomenon known as the resonance condition happens when the magnetic field and microwave frequency are "just right" (*i.e.*, the energy of the microwaves matches to the energy difference of the pair of involved spin states). Allowed EPR transitions occur when $\Delta M_s = \pm 1$, where M_s is the magnetic spin quantum number of the spin state.The following equation describes the transfer of microwave energy ΔE between two spin states:

$$\Delta E = h\nu = g\beta B \tag{2.4}$$

where, ΔH = Energy difference between the two spin states, h = Planck constant, ν = microwave frequency, g = Zeeman splitting factor (Lande g-factor), β = Bohr magneton

EPR spectroscopy acquires an absorption spectra by using a constant radiation frequency in contrast to the majority of traditional spectroscopy techniques. X-band ESR spectra were captured for this thesis utilizing a JEOL, Japan (Model: JES-FA200 ESR) spectrometer. Low microwave power and a 100 kHz magnetic field modulation were utilized to prevent saturation effects. Liquid N_2 was used as a coolant while collecting low-temperature ESR spectra. The external magnetic field was used to gather the first derivative of the absorption spectra.

2.2.8 Magnetic property measurement system (MPMS)

The magnetic property measurement system (MPMS) is a sophisticated technology for measuring the magnetic moments of small magnitude in powder, single crystals, thin films, pallets, and so on over a wide range of temperatures and under applied external magnetic fields. The magnetization measurements in our research were carried out with the Quantum Design Magnetic Property Measurement system, also known as **"MPMS"**. The model MPMS3 allows us to measure magnetization in the temperature range 1.8 K to 400 K using liquid He-based cryostat and magnetic field range $\pm$ 7.0 T with several measurement options. This magnetometer has a very high sensitivity (10^{-8} emu) and an easy-to-use control system. The magnetic moments are measured in this instrument with the help of vibrating sample magnetometer (VSM) and the superconducting quantum interference device (SQUID). The working principle of both VSM and SQUID is provided below.

VSM

According to Faraday's law, a change in the magnetic moment of the sample changes slightly, it induces a voltage in a series of detection coils. The induction technique is used to measure induced voltage that involves vibrating the specimen at a constant frequency in a uniform magnetic field.

In practice, the VSM operates at temperatures ranging from 2 to 400 K and with a magnetic field of ± 7 T. The magnetic moment is precisely quantified by measuring the induced voltage at the detecting coils. The detecting coils are contained within a solenoid, which generates the magnetic field. The VSM is predicated on the existence of multiple magnetic dipoles in a specimen. At the beginning of the measurement, the specimen is positioned in the middle of the detection coil. When it is displaced in time (t), the change in flux (ϕ) induces a voltage, which is given by v = dϕ/dt. This voltage is detected in the detection coils, and the subsequent moment in the specimen is measured in relation to the applied magnetic field.

The VSM is capable of maintaining excellent accuracy in measuring the magnetic moment of the specimen. This is due to the induction method used, which allows for the measurement of even slight changes in the magnetic moment.

SQUID magnetometry

For measuring the minute magnetic moment in the specimen, SQUID is the most suitable and sensitive technique. The core part of a MPMS is the SQUID sensor and highly sensitive magnetometer which is commonly used for this purpose. The SQUID sensor is made up of two parallel Josephson Junctions, which are weak connections between two superconductors divided by thin insulating layers. The Josephson effect, discovered by B.D. Josephson in 1962, enables a supercurrent to flow continuously through the weak link without any voltage across the Josephson junction via Cooper pair tunnelling. The tunnelling action of Cooper pairs across a Josephson junction of two superconductors separated by an insulating gap is the working concept of the SQUID magnetometer [91]. The maximum critical value of this supercurrent is known as IC. A superconducting ring with two Josephson Junctions is the heart of SQUID.

The SQUID sensor has a superconducting ring, which permits only a magnetic flux whose magnitude is an integral multiple of ϕ_0 = h/2e = 2.07×10^{-15} T-m^2 (the flux quantization in superconductors) to pass through it. Any change in magnetic flux through the loop induces a screening current in the superconducting ring to maintain flux quantization. The small magnitude of ϕ_0 allows for the development of an extremely sensitive magnetic

sensor like the SQUID. Using SQUIDs, magnetic flux related to any material can be converted to a voltage signal, thanks to the flux quantization sensitivity in superconductors. The SQUID is also known as a flux-to-voltage transducer because it can transform a very small change in magnetic flux into a voltage signal. The critical current through the superconductor changes when an external magnetic field of any material enters the ring. This shift in current is amplified to a voltage signal by electronic devices calibrated to determine the magnetic moment of the system. In summary, the MPMS's SQUID sensor detects changes in the critical current flowing through the superconductor in reaction to an external magnetic field. The resulting voltage signal is amplified and calibrated to provide the magnetic moment of the device under investigation. The possible mode of magnetization measurements was described further.

dc magnetization

Direct current (dc) magnetometry is a popular technique for determining the magnetization (**M**) of magnetic materials in which a constant magnetic field is applied to the sample and the magnetic moment is measured using either induction or torque techniques. The equilibrium value of the magnetic moment is obtained by maintaining a constant magnetic field during the measurement. The magnetic flux density (**B**) is measured as a function of the magnetic field intensity (**H**), and the magnetization is calculated using the equation $B = \mu_0(H+M)$, where μ_0 is the permeability of free space. The change in magnetic susceptibility (χ_{dc}) with respect to the applied magnetic field strength is also measured, which is the proportionality constant between the magnetization and the applied magnetic field, valid only in the paramagnetic phase. As a matter of fact, the paramagnetic state transforms into ferro/antiferro magnetic state with temperature variation known as magnetic transition. The transition temperature where the paramagnetic state converts into ferro/antiferro magnetic state is known as Curie/Neel temperature, respectively. This transition temperature was described by the Curie-Weiss law or cusp of the first derivative of magnetization with temperature. The Curie-Weiss law is given by:

$$\chi = \frac{C}{T - \theta} \tag{2.5}$$

where C is the Curie constant, T is the absolute temperature in kelvins, and θ is Curie-Weiss temperature, related to the exchange interaction between magnetic moments, a positive value indicates ferromagnetic (FM) ordering, negative for antiferromagnetic (AFM) ordering, and zero for exclusively paramagnetic. The first derivative of dc magnetization and temperature defined different magnetic transition.

ac magnetization

ac magnetic measurements entail superimposing an ac drive magnetic field on a dc field and measuring the sample's time-dependent ac moment. This technique gives valuable information on magnetization dynamics that dc magnetometry does not, because the sample moment remains constant during the measurement. At very low frequencies, ac susceptibility is similar to dc, but its frequency dependence gives additional information about the magnetic nature of the sample. Due to dynamic effects, the ac moment of the sample deviates from the dc magnetization trajectory at higher frequencies, and ac is thus referred to as dynamic susceptibility.

The χ_{ac} measurement yields two distinct quantities, defined as $\chi_{ac} = \chi^{'} - i\chi^{''}$, where $\chi^{'} = \chi \cos(\phi)$, $\chi^{''} = \chi \sin(\phi)$, and $\phi = \arctan(\chi^{''}/\chi^{'})$. The magnitude of χ_{ac} is given by the square root of the sum of the squares of the real and imaginary components. The phase shift (ϕ) represents the relative timing between the ac drive field and the resulting ac moment of the sample.The real component $\chi^{'}$ is the in-phase component, and represents reversible magnetization processes, while the imaginary component $\chi^{''}$ is the out-of-phase component, and represents dissipative or irreversible magnetization processes. In conductive samples, the dissipation is due to eddy currents, while in spin-glass systems, relaxation and irreversibility give rise to a nonzero value of $\chi^{''}$. A nonzero imaginary susceptibility in FM and AFM materials can denote permanent moment-induced domain wall movement or irreversible absorption.

Both $\chi^{'}$ and $\chi^{''}$ are sensitive to thermodynamic phase transitions and can be used to measure transition temperatures. ac magnetometry enables the probing of these phenomena by measuring χ as a function of the frequency, temperature, dc field bias, ac field amplitude, and harmonics.

We have measured magnetization as a function of temperature, field, and ac frequency in our research. The training effect followed the exchange bias and spin glass characteristics, which were then measured along with memory and rejuvenation. The various protocols were utilized for magnetization measurement, details are given below:

• Zero field cooling (ZFC): The magnetization *w.r.t.* temperatures and field measured in ZFC mode. The sample was cooled to a low temperature (300 K to 5 K) without the presence of a magnetic field, after then a small magnetic field (100 Oe) is applied in a fixed orientation to the sample, and magnetization measurements were taken while sweeping the temperature from 5 K to 300 K. In the case of magnetization vs field (M-H loop) measurement sample was cooled at a particular temperature after the magnetization measure with respect to the variable field presence.

• **Field cooling (FC):** Magnetization in relation to temperature and field observed in FC mode. The sample was cooled to a low temperature in the presence of a certain field, and data were collected as the sample's temperature raised. The sample was subjected to cooling to a particular temperature in a steady magnetic field.The field was turned off at a specific temperature, and magnetization was recorded in relation to the variable field presence.If magnetization recorded during cooling, then it's known as filled cooled cooling (FCC), or in warming, filled cooled warming (FCW).

Few of these will be discussed in the next upcoming chapters.